Robust Biosensor Based on Carbon Nanotubes/Protein Hybrid Electrolyte Gated Transistors

Robust Biosensor Based on Carbon Nanotubes/Protein Hybrid Electrolyte Gated Transistors

Alessandro Paradisi,[a] Marcello Berto,[a] Matteo Di Giosia,[b] Sara Mazzali,[a] Marco Borsari,[c] Tainah Dorina Marforio,[b] Francesco Zerbetto,[b] Matteo Calvaresi,[b] Anna Orieshyna,[d] Nadav Amdursky,[d] Carlo Augusto Bortolotti,[a] Fabio Biscarini*[a,e]*

[a] Dr. A. Paradisi, Dr. M. Berto, Sara Mazzali, Prof. C. A. Bortolotti, Prof. F. Biscarini
Department of Life Sciences
University of Modena and Reggio Emilia
via Campi 103, 41125 Modena (Italy)
E-mail: alessandro.paradisi@unimore.it, fabio.biscarini@unimore.it

[b] Dr. M. Di Giosia, Dr. T. D.Marforio, Prof. F. Zerbetto, Prof. M. Calvaresi
Chemistry Department "Giacomo Ciamician"
Alma Mater Studiorum University of Bologna
Via Francesco Selmi 2, 40126 Bologna (Italy)

[c] Prof. M. Borsari
Department of Chemical and Geological Sciences
University of Modena and Reggio Emilia
Via Campi 103, 41125 Modena (Italy)

[d] A. Orieshyna, Prof. N. Amdursky
Schulich Faculty of Chemistry
Technion–Israel Institute of Technology
3200003 Haifa (Israel)

[e] Prof. F. Biscarini
Center for Translational Neurophysiology
Istituto Italiano di Tecnologia
Via Fossato di Mortara 17-19, 44121 Ferrara (Italy)

Abstract: Semiconducting single walled carbon nanotubes (SWCNTs) are promising materials for biosensing applications with electrolyte-gated transistors (EGT). However, to be employed in EGT devices, SWCNTs often require lengthy solution-processing fabrication techniques. Here, we introduce a simple solution-based method that allows fabricating EGT devices from stable dispersions of SWCNTs/bovine serum albumin (BSA) hybrids in water. The dispersion is then deposited on a substrate allowing the formation of a SWCNTs random network as the semiconducting channel. We demonstrate that this methodology allows the fabrication of EGT devices with electric performances that allow their use in biosensing applications. We demonstrate their application for the detection of cortisol in solution, upon gate electrode functionalization with anti-cortisol antibodies. This is a robust and cost-effective methodology that sets the ground for a SWCNT/BSA-based biosensing platform that allows overcoming many limitations of standard SWCNTs biosensor fabrications.

Introduction

Electronic and electrochemical biosensors are devices that leverage the transduction of biochemical events happening on electrode surfaces into electric signals. Recent advances in this field showed that they can be integrated into flexible devices, and low-power consumption circuits,[1,2] with the added advantage of direct interfacing capabilities with biological fluids and tissues.[1,3,4] Additionally, recent works have demonstrated the possibility to integrated them with artificial intelligence software, opening up new avenues to enhance data acquisition and analysis.[5,6]

In this context, electrolyte-gated transistors (EGTs) are a promising class of electronic devices that gained significant attention in recent years. This attention stems from their intrinsic signal amplification capabilities, resulting in exceptionally high sensitivity, as well as their ability to operate directly in aqueous environments. In fact, EGTs are characterized by a low operating voltage (< 1 V) thanks to the formation of an electric double layer (EDL) with high capacitance (> 1 μF cm^{-2}) at the electrode/electrolyte interface, when the gate electrode is polarized.[1,7] Historically, EGTs have been categorized into two distinct groups based on the ionic permeability of the semiconducting material employed. In the first category, known as electrolyte-gated field effect transistors (EG-FETs), the ionic interaction occurs solely at the interface between the electrolyte and the semiconductor (*via* the formation of the EDL). Conversely, the second category consists of EGTs, with ion-permeable semiconductors where the ionic-electronic

interaction takes place throughout the three-dimensional volume of the active material. These devices are generally referred to as electrochemical transistors.

Semiconducting single walled carbon nanotubes (SWCNTs) represent promising semiconducting materials for EGT devices based on the FET operation mode (sometimes also referred as EG-CNTFETs).[8,9] SWCNTs have excellent electrical conductivity, even at low applied voltages (< 1 V), and stable in air and aqueous environments.[10–12] Furthermore, the one-atom-thick structure of SWCNTs makes them one-dimensional materials where each carbon atom is in contact with the surrounding environment, hence making electrical properties very sensitive to changes in this environment.[11,13] However, the processing of SWCNTs into useful forms for EGT applications, such as thin films and composite materials, presents several challenges; especially when it comes to solution processing because of their low solubility in most solvents and their tendency to form aggregates in solution.[10,12,14] Because of their high surface/aspect ratio, carbon nanotubes typically form ropes and bundles of 10–30 nm in diameter driven by the strong van der Waals forces between the individual tubes. Such bundles can significantly hamper the SWCNTs' electric properties in EGT applications;[15] therefore, achieving stable dispersions in a solvent is a crucial step for SWCNTs solution processing.

Ultrasonication and shear force mixing procedures are generally applied to disperse SWCNTs in solution reducing the dimension of the bundles, together with their chemical functionalization, to stabilize the dispersions.[16–19] Non-covalent functionalization methods are widely exploited since they allow to preserve the electronic properties of the nanotubes and can be carried out using a wide variety of polymers, surfactants, and (poly)peptides.[20–22] In particular, it has been shown that several proteins can bind the SWCNTs surfaces through non-covalent interactions like hydrophobic and π–π interactions and allow the use of water as solvent.[22–24] Hence, the possibility to prepare water-based solutions of SWCNTs makes the use of proteins an interesting possibility towards simple, low-cost, and green processing methods.

Water-based solutions of SWCNT/lysozyme adducts can be used to fabricate EGT devices with good performances and stability when operating in electrolyte solutions.[25] In biosensing applications, after deposition on suitable substrates, SWCNTs are generally functionalized with enzymes, antibodies, or aptamers, to confer sensitivity towards a particular target molecule.[19,21,26] Furthermore, a recent work from Bisker *et al*. demonstrated the possibility to functionalize SWCNTs with a synthetic non-biological antibody analogue for the specific detection of proteins in solution.[27] These approaches typically exploit the presence of carboxylic acid moieties on the nanotubes surface defects for the covalent binding of antibodies *via* amide bond formation.[19] However, this requires chemical modification of the SWCNTs which may alter their π-conjugated ring system and, as a consequence, their electronic properties.[14] Alternatively, a second common strategy is to use a bifunctional reagent like 1-pyrenebutanoic acid succinimidyl ester that has on one side a pyrene group (that adsorbs on the SWCNT side wall through π–π stacking interactions) and on the other side an active ester group for covalent binding to the amine moieties of antibodies.[28] However, these strategies are not necessarily compatible with the functionalization methods required for the de-bundling of SWCNTs and their deposition on the substrate. Therefore, it would be important to couple the ease of deposition *via* SWCNT/protein hybrids dispersions with the flexibility of using the relevant antibodies to achieve high reproducibility in the device fabrication and statistical robustness of the biosensor response. In addition, an important problem to face in biosensing is the non-specific adsorption at the semiconductor-electrolyte or gate-electrolyte interfaces that may be disguising the actual signal from the biological target. Accordingly, there is a need to implement measurement protocols that minimize the biosensor response to non-specific binding events.

In this work, we show a simple, low-cost, and robust method to fabricate EGT biosensors based on SWCNTs/protein hybrids. For the protein, we chose bovine serum albumin (BSA), which is one of the most commercially affordable proteins. Most importantly, BSA can easily solubilize a variety of molecules, thus preventing their solution-induced aggregation, and if the chosen molecule is conductive, it can form conductive materials.[29,30] Here, the BSA was used to prepare stable dispersions of SWCNTs in water.[31] We demonstrate that the dispersion can be used to fabricate EGT devices and that, upon functionalization of the gate electrode with monoclonal anti-cortisol antibodies, the device can be used to detect cortisol in aqueous solutions. Cortisol is a steroid hormone involved in the regulation of various physiological processes, including metabolism, stress response, and immune function.[32] Cortisol is produced by the adrenal gland in response to stress and other physiological stimuli. Abnormal levels of cortisol were associated with various disorders, including Cushing's syndrome, Addison's disease, and depression.[33,34] Therefore, the development of reliable and accurate methods for measuring cortisol levels is crucial for early diagnosis and effective management of these conditions. Cortisol biosensors offer a promising solution to this problem,[35–37] providing a rapid and non-invasive means of measuring cortisol levels in biological fluids such as blood, saliva and sweat.[33,38–42] However, because of its very low concentration in these fluids, highly sensitive devices are needed for efficient quantification, making EGTs promising candidates for this application. Thanks to the high transconductance of the SWCNTs/BSA-based transistors we were able to quantify the concentration of cortisol in the 10–1000 pM concentration range in solution, with an estimated limit of detection (LOD) of 0.6 pM.

Results and Discussion

Interaction between BSA and (6,5) SWCNTs

Surface complementarity between BSA and the (6,5) SWCNTs surface allows the supramolecular dispersion of the tubes. BSA perfectly surrounds the CNT walls. A docking protocol developed to identify the interaction site between proteins and carbon nanotubes identified four possible binding sites of (6,5) SWCNTs in BSA (Figure S1a). Molecular Dynamics (MD) simulations followed by MM-GBSA estimated the binding energy between the tube and the different binding pockets of the protein (Figure S1b). The favourite position for the tube is in BSA cleft region between the Domains I and III. An alternative location for the tube pass through Domain I and II (Figure 1).

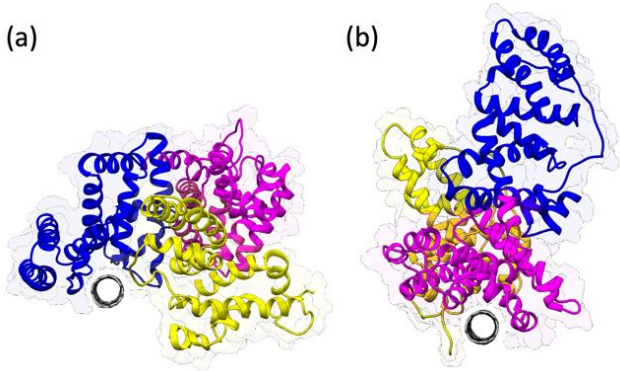

Figure 1. Interaction between BSA and a (6,5) SWCNT. Cartoon representation of the secondary structure of the protein (domain I, yellow; II, magenta; III, blue), while the protein surface is represented as transparent surface**.** (a) Favourite (6,5) SWCNT binding site between domain I and III. (b) Secondary binding site passing through Domain I and II.

The driving force for the binding (Figure S1b) is due to van der Waals interactions. Hydrophobic interactions, *i.e.*, nonpolar solvation, also favour the binding, while polar solvation is detrimental. The binding of the CNT occurs in regions of the protein exposed to water and where polar amino acids are commonly found. The hydrophilic side chains, upon CNT binding, are forcedly desolvated and hence destabilizing the system. Overall, shape complementarity and hydrophobic effect governs the interaction between the (6,5) SWCNT and BSA.[31] At an atomistic level (Figure S2), the BSA binds the nanotube surface with several amino acids through non-covalent interactions, like π–π (Tyr496, His3, Phe325), hydrophobic (Leu505, Val497, Val228, Pro96) and surfactant-like (Thr419, Gln416, Lys64), interactions, and therefore stabilizing the SWCNTs' dispersions in water.[23]

Electrolyte Gated Transistor Characterization

The SWCNT/BSA adducts were prepared by ultrasonication of the semiconducting SWCNT powder with a solution of BSA in H_2O. The obtained dispersion was centrifuged to remove the undissolved solid.
The resulting grey-black coloured solution was then characterized with UV-vis spectroscopy. The UV-vis spectrum presents two main absorption bands at 996 nm and 576 nm that correspond to the first two electronic transitions of the (6,5) SWCNTs, due to van Hove singularities in the 1D density of states, namely E_{11} and E_{22} respectively (Figure2a).[43,44] The very intense absorption around 280 nm is due to absorption from the BSA in the solution. In addition, and in accordance with the SWCNTs used, the spectrum also exhibits additional absorption bands with lower intensities, which are probably due to nanotubes with different diameters and chirality and therefore with different electronic transition energies.
The SWCNT/BSA hybrids solution was then drop-cast onto gold interdigitated source-drain electrodes (Figure S3) to fabricate the semiconducting channel of the transistor through the formation of a SWCNT random network. This material was further characterized with Raman spectroscopy. The Raman spectrum of the SWCNT/BSA random network shows several vibrational bands in the low energy region which are characteristics of the carbon nanotubes radial breathing modes (RBMs, Figure2b).[45] The energy of these modes is inversely proportional to the tube diameter; therefore, the spectrum is consistent with the presence of nanotubes with slightly different diameters, around 0.75–0.80 nm. At higher energies, the vibrational spectrum is dominated by the so-called *G* (1591 cm^{-1}) and *D* band (1303 cm^{-1}) of the SWCNTs (Figure2c); in particular, the *G*-band shows a sharp and symmetric line shape consistent with the absence of significant contamination from metallic carbon nanotubes.[46]

Atomic Force Microscopy (AFM) characterization of the surface demonstrates the formation of a random network of nanotubes with small bundles of SWCNT/BSA adducts and an average height of 30–50 nm. A single carbon nanotube (average length of ~1 µm) is not long enough to bridge the 15 µm gap of the interdigitated electrodes, therefore the formation of a random network allows electronic charge percolation through multiple pathways formed by connected nanotubes between the source and drain electrodes. AFM topography showed that the SWCNT/BSA adducts are evenly distributed over the substrate although they do

not cover it completely, leaving bare channel and electrode regions exposed to the electrolyte (indicated as darker areas in Figure 3).

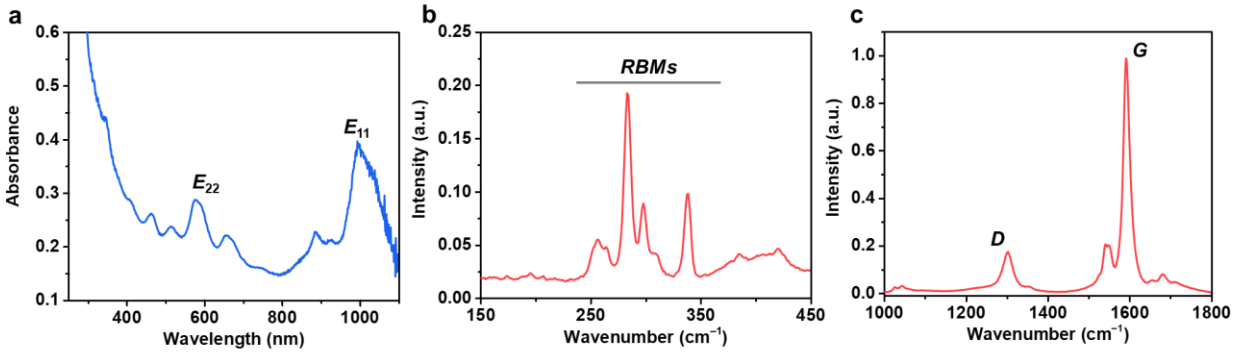

Figure 2 (a) UV-vis spectrum of the SWCNT/BSA solution in water. The E_{11} (996 nm) and E_{22} (576 nm) labels indicate the electronic transition assigned to the (6,5)-carbon nanotubes. Raman spectrum, collected with laser excitation at 633 nm of the SWCNT/BSA random network deposited on the substrate: (b) low energy region showing the radial breathing modes and (c) higher energy region showing the SWCNT characteristic *G* (1591 cm^{-1}) and *D* (1303 cm^{-1}) bands.

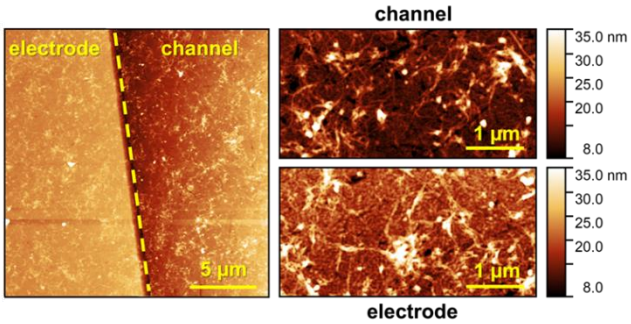

Figure 3 AFM topography of 20×20 µm areas of the (left) Au electrode and SiO_2 substrate of the channel of the transistor, highlighting the SWCNT/BSA random network on top of the substrates. (right) 5×5 µm expanded view of the channel (top) surfaces and Au electrode (bottom). The coloured scale on the side of the figures indicates the heights of the surface features.

The SWCNT/BSA random network was then integrated into a device with a top-gate bottom-contact transistor architecture. The electrical characterization of the transistor was performed with a 50 mM phosphate buffer as the gating electrolyte, contained in a PDMS pool placed above the test pattern; a gold wire was used as a gate electrode to complete the EGT device. Representative characteristics for these devices are reported in Figure 4, showing a *p*-type behaviour with drain-source currents (I_{DS}) reaching ~8–9 µA at –600 mV applied at the gate (V_{GS}) and with a threshold voltage $V_{th} \approx -450$ mV. The transconductance value (g_m) showed in Figure 4b, is already one order of magnitude larger than typical values obtained with organic semiconductor channel in EG-FET transistors.[47,48] This is a noteworthy result since g_m can be increased upon getting a better coverage of the SWCNT/BSA network, as the highly porous percolation SWCNT/BSA network covers only a fraction of the electrode interdigitation (as shown by the AFM imaging of the channel, Figure 3). The transconductance magnitude is a hallmark of the ionic-electronic interaction in EGTs. Even though EGTs composed of denser networks of highly pure (6,5) SWCNTs generally exhibit higher measured transconductance (g_m),[9,49] ours results demonstrate that a simple and fully water-based fabrication procedure can yield an SWCNTs-based device with good performances, if compared to EGT devices based on organic semiconductors. The current *on*/*off* ratio is in line with that of organic semiconductors in EGTs and is mainly limited by the sizable I_{DS} in the *off* state (tens of nA) which could arise from significant leakage current due to the exposure of the source electrode to the electrolyte. Noticeably, the transistor output characteristics show a well-defined linear behaviour at $V_{DS} > -100$ mV, which tends towards a saturation regime at more negative potentials (Figure S4). The linear behaviour at small applied V_{DS} is consistent with an efficient charge injection due to low contact resistance.

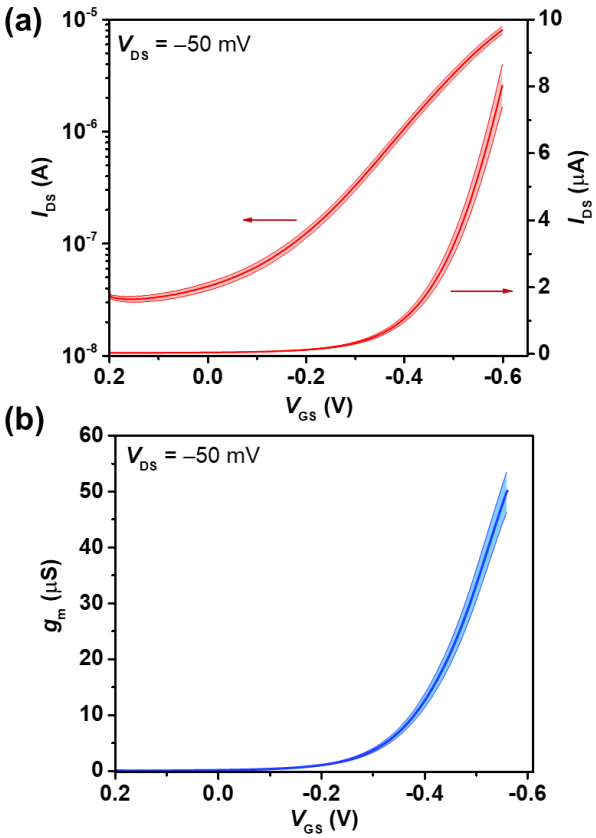

Figure 4 (a) Average transfer characteristics (number of independent channels *n*=15) of the SWCNT/BSA EGT device in both semi-log and linear scale, using bare gold gate electrodes. (b) Transconductance curve obtained from the average transfer curve in (a). Shaded areas in both plots represent the standard error associated with the average curves.

Stability over time is an important feature for electronic devices used in biosensing applications.[9] Hence, the stability of the electronic performances of the of SWCNT/BSA channel operating in phosphate buffer electrolyte was evaluated over time, using a an Ag/AgCl electrode as gate (as this electrode is generally considered very stable in aqueous environments). A series of successive transfer curves with interval of 5 min between each other were collected over a 4.5 h period.[9] The stability was evaluated as current I_{DS} shift relative to the initial current at fixed gate applied potential ($-(I-I_0)/I_0$, where I_0 is the current measured at 0 min). As shown in Figure S5, the I_{DS} undergoes a significant change during the first 130–150 min and then stabilizes, with only small oscillations of about ±1% over the following two hours.
Overall, the analysis of the electrical properties demonstrates the possibility to produce a working EGT with good performance following a very straightforward fabrication procedure using BSA to disperse SWCNT in water.

Cortisol Sensing

To assess the suitability of our EGT as the base for a biosensing platform, we developed a biosensor for cortisol in solution. To confer sensitivity to the target molecule, the gold gate electrode was functionalized with anti-cortisol monoclonal antibodies. The functionalization procedure consisted in growing a self-assembled monolayer (SAM) of a 11-mercaptoundecanoic/6-mercaptohexanol mixture (1:3 molar ratio, respectively). The monoclonal antibodies were then covalently bound to the SAM carboxylate functional groups *via* EDC/NHS amide bond coupling (see Experimental Section for details). The formation of the cortisol bioreceptor layer on the gold surface was characterized with cyclic voltammetry and electrochemical impedance spectroscopy using $[Fe(CN)_6]^{3-}/[Fe(CN)_6]^{4-}$ as a redox probe (Figure S6). Upon functionalization of the electrode surface with the antibody layer, the charge transfer resistance between the redox probe and the electrode was increased, which reduced the faradaic current recorded with respect to the bare gold electrode.

In the biosensing experiment, the functionalized gate electrode was exposed to standard solutions of cortisol dissolved in phosphate buffer 50 mM pH 7.4, which were also acting as the gating electrolyte for the transistor. The cortisol concentration range tested was from 1 pM to 1 μM. Each EGT device was first stabilized by cycling with successive transfer curves as reported above, and then used for the biosensing experiment. For each sample, consecutive transfer curves were collected until stabilization of the drain current; this procedure allows the analysis of the transistor response under the hypothesis that the binding

of the analyte to the gate electrode has attained thermodynamic equilibrium. Figure 5a shows a typical response of the EGT transfer characteristics measured in the linear regime of the transistor (V_{DS} = –50 mV): an increasing concentration of cortisol leads to a reduction of the recorded I_{DS}.

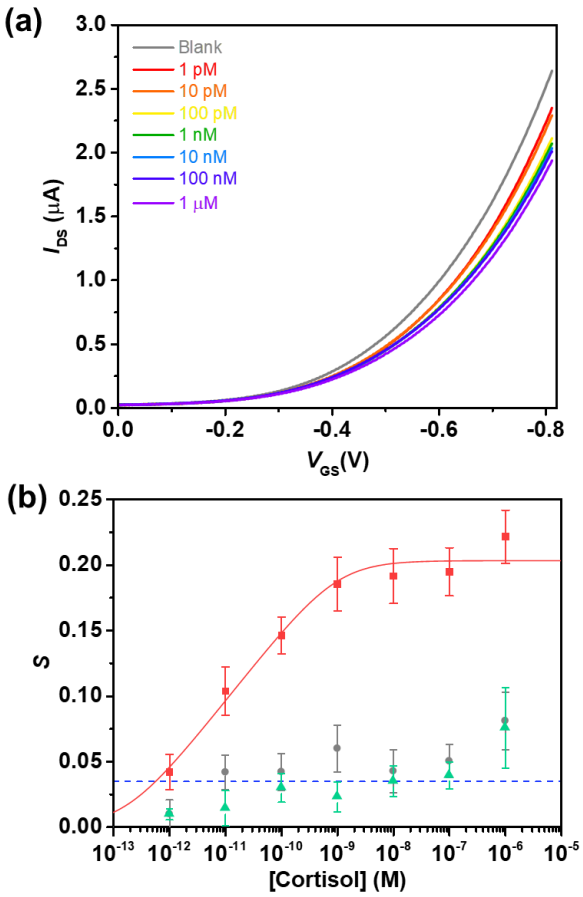

Figure 5 (a) Representative transfer curves showing the response of the SWCNT/BSA electrolyte-gated transistor to different concentrations of cortisol in 50 mM phosphate buffer at pH 7.4, V_{DS} = –50 mV. (b) Calibration curves obtained with the measured signal *S* at V_{GS}= –0.8 V. Red squares represent the response where the gate was functionalised with anti-cortisol antibodies, together with the associated uniform Langmuir isotherm fitting. The grey dots represent the control samples, where the gate electrode was functionalized with antibodies not specific for cortisol. The green triangles represent the control samples where the gate electrode was functionalized only with the self-assembled monolayer but without antibodies. Lastly, the blue dashed line represents the theoretical LOD, estimated by taking three times the I_{DS} (at V_{GS}= –0.8 V) standard deviation of the blank sample. Errors associated with the data points are reported as standard errors.

To quantify the biosensor response to variations of analyte concentration, a titration curve was built by plotting the signal (*S*) recorded against cortisol concentration. The signal is defined as the normalized current variation with respect to the blank sample: $S = -(I-I_0)/I_0$; where *I* is the current (I_{DS}) measured at a fixed gate potential and I_0 is the current measured at the same gate potential in the blank sample. The signal was initially calculated at different gate potentials, giving similar results as a function of cortisol concentration. Finally, the calibration curve was obtained with I_{DS} values extracted at V_{GS} = –800 mV, because at this potential the calculated *S* showed a smaller standard error with respect to the other V_{GS} potentials and hence best reproducibility. The biosensor signal (*S*) shows a non-linear monotonic trend as a function of analyte concentration, which leans toward saturation at cortisol concentration higher than 1 nM; this saturation corresponds to a maximum I_{DS} drop of ~20% with respect to the initial value in the absence of cortisol (Figure 5b).

To verify that the measured signal was due to the specific binding of cortisol to the monoclonal antibodies on the gate electrode surface, two different control experiments were performed. In the first one, the gate electrode was functionalized only with the SAM, and the signal was again extracted for V_{GS} = –0.8 V as a function of cortisol concentration. The result (Figure 5b, green triangles) shows that the recorded signal is significantly lower than the one recorded with the anti-cortisol antibodies, and it is in the order of the estimated limit of detection (LOD) (see below discussion). A second control experiment was performed by functionalization of the SAM with antibodies non-specific for cortisol. In this case, after an initial increase, *S* already saturates for concentration higher than 10 pM, with a ~5% shift with respect to the initial I_{DS} values (Figure 5b, grey dots). Together, the control experiments suggest that a small fraction of the signal recorded in the normal calibration curve is possibly due to non-specific interactions of the cortisol with the gate electrode surface (when it is decorated with antibodies), and likely not due to interactions

with the SWCNT/BSA channel. However, this contribution remains very small and essentially constant with respect to increasing concentration of cortisol and hence does not preclude the sensing of cortisol by the functionalized electrode. Furthermore, the signal recorded at the highest concentration tested (1 µM) is systematically higher with respect to the plateau recorded for the 1–100 nM range, both in the calibration curve and in the control experiments. This behaviour could be explained by considering that at 1 µM cortisol is close to its maximum solubility in aqueous solution, so there could be formation of cortisol aggregates on the gate and/or channel surfaces. An alternative explanation is that the amount of leftover DMF solvent from the dilution of the cortisol stock solution is not negligible anymore, hence it affects the EGT electrical properties. However, this concentration is generally much higher with respect to the standard cortisol physiological range (0.01–100 nM), hence a small contribution from non-specific interactions at the µM concentration range should not represent a significant problem.

Two of the major mechanisms that allow sensing in electrolyte-gated transistors are the change in gating effective capacitance of the electric double layer (EDL) and/or a shift in the device threshold voltage.[1,7,50] In this case, the recorded decrease of I_{DS} current is always accompanied by a decrease in transconductance g_m (Figure S7). If the detected signal is quantified in terms of normalized transconductance change as a function of cortisol concentration ($S_{gm} = -(g_m - g_{m0})/g_{m0}$), the obtained calibration line follows the same trend observed for I_{DS}, as shown in the S_{IDS} vs S_{gm} correlation plot (Figure 6a). On the other hand, the threshold voltage tends to shift towards slightly more negative gate voltages with increasing concentration of cortisol, but this shift (ΔV_{th}) always remains small (less than 5 mV, Figure S8) and likely does not contribute significantly to the drop in I_{DS} as a function of cortisol concentration.

Considering the standard model for the EGT working mechanism, the transconductance g_m is proportional to the product of the charge carriers mobility μ and the capacitance. The carrier mobility in SWCNT random networks is generally high (1–1000 $cm^2 V^{-1} s^{-1}$) and can only be significantly altered as a consequence of drastic changes to the nanotube electronic structure. In fact, Heller *et al*. reported that even when the protein binding events happen directly on the SWCNT surface, the perturbation was not enough to produce significant change in nanotubes mobility.[50] Hence, if charge carrier mobility does not undergo sizable changes upon cortisol binding at the gate electrode, the changes of g_m upon biorecognition events can be mainly associated with changes in the capacitance.[19,50]

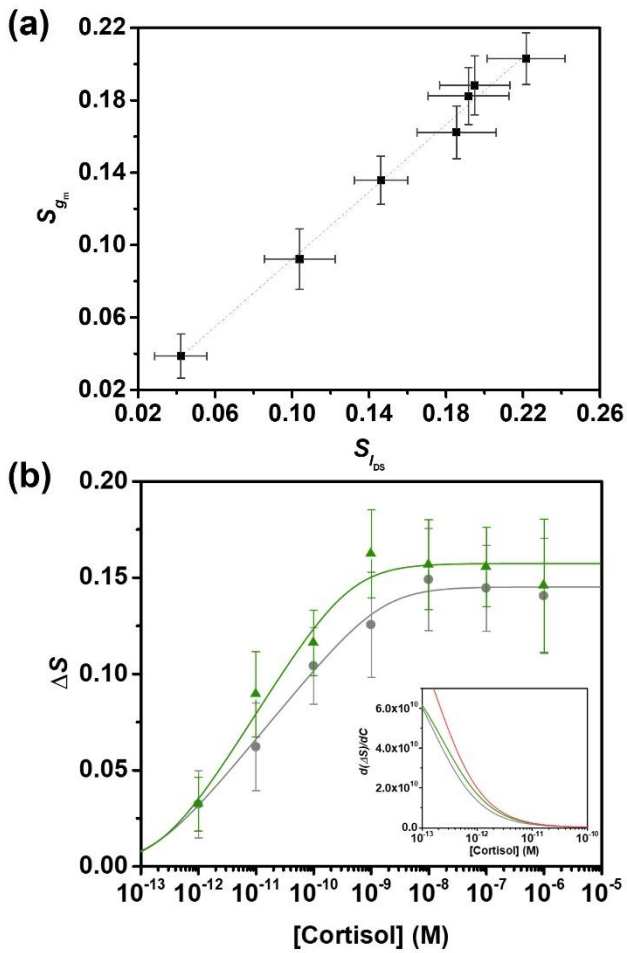

Figure 6 (a) Correlation plot of the normalized I_{DS} change (S_{IDS}) against the normalized g_m (S_{gm}) change, at each cortisol concentration, calculated at V_{GS}= –0.8 V, with associated standard errors. (b) Signal difference between the cortisol calibration curve (Figure 5) recorded with the gate electrode functionalized with anti-cortisol antibodies and gate electrodes for the control experiment, functionalized with: antibodies non-specific for cortisol (grey dots) or functionalized

with SAM only (green triangles). The associated standard errors were calculated by error propagation of the subtraction operation between the two data sets. Fitting lines for each experimental curve were calculated with the uniform Langmuir Model. Inset: the slope of the fitting curves for the calibration line using the gate electrode functionalized with anti-cortisol antibodies (red) and for the calibration lines using the ΔS with calculated with control electrodes with antibodies non-specific for cortisol (grey) or functionalized with SAM only (green).

Under the assumption of thermodynamic equilibrium between bound and free cortisol in solution, the non-linear response of the biosensor can be analysed in terms of equilibrium binding models (isotherms) in order to obtain a calibration curve for the biosensor. In this context, two of the most used models are the Langmuir and the Hill isotherm (Table S1). However, the Langmuir isotherm does not reproduce well the non-linear trend of the experimental data (Figure S9), as it requires reaching saturation in a narrower concentration range with respect to the one observed experimentally. On the other hand, the Hill isotherm better follows the experimental trend thanks to the introduction of an additional empirical parameter α generally interpreted as cooperative ($\alpha > 1$) or non-cooperative ($\alpha < 1$) binding of the receptor towards its target.[51] However, an alternative interpretation can be given in terms of simultaneous multiple equilibria involving the ligand, the target, and the bound pair at the electrode surface. It has been demonstrated that the value of α can take values lower or higher than 1, where multiple equilibria can effectively increase or decrease the dependence on the concentration with respect to a Langmuir-type process ($\alpha = 1$).[51–53]
An alternative hypothesis considers a generalization of a multi-sites Langmuir model by considering the presence of a large number of binding sites on the electrode surface, with different binding energies (U), that are uniformly distributed in the range $U_{min} < U < U_{max}$.[54,55] If adsorbate-adsorbate interactions are neglected, as in the standard Langmuir model, the resulting isotherm follows the distribution of binding energies among the adsorption sites. This model is generally referred to as a uniform Langmuir model:[54]

$$S = \frac{S_{max}}{2A} ln\left(\frac{1 + K_{avg}\, e^{A}\, c}{1 + K_{avg}\, e^{-A}\, c}\right)$$

where A is a parameter defined as follows:

$$A = \frac{1}{2\, k_B T}(U_{max} - U_{min})$$

S_{max} is the maximum signal recorded, corresponding to the saturation of the binding sites, K_{avg} is the average binding constant (corresponding to a Langmuir constant of a hypothetical material with uniform adsorption sites), c is the concentration, k_B is the Boltzmann constant, and T is the temperature.
In this case, the variety of different binding sites can be explained by considering the gate electrode surface being heterogeneous because of the random orientation of the antibodies covalently linked to the 11-MUA and the possible formation of antibodies aggregates with different dimensions due to the heterogeneous distribution of the 11-MUA molecules in the SAM.
This model allows us to reproduce well the concentration dependence of the signal recorded (Figure 5b) and to extract an estimated value for $K_{avg} = (8\pm1)\times10^{10}$ for the binding of cortisol to the gate electrode, with the coefficient $A = 4.3 \pm 0.6$, which corresponds to a binding difference $U_{max}–U_{min} = 21 \pm 3$ kJ/mol, between the site with highest and lowest affinity (Table S1).
The theoretical LOD was estimated on the basis of the transfer curve standard deviation of a blank sample (*i.e.* in the absence of cortisol). Following the IUPAC convention[56], the LOD was defined as the concentration of cortisol that corresponds to a signal of $S_0 \pm 3\sigma$, where S_0 is the signal of the blank which in this case is set to zero, and σ is the standard deviation of the signal of the blank sample. By propagation of the error, we obtain $\sigma = 2\delta I_0/I_0$, where δI_0 is the I_{DS} standard deviation of the blank sample. Its value was estimated as $\sigma = 0.011$, which returns a theoretical LOD of 0.6 pM based on the uniform Langmuir isotherm fit presented in Figure 5b and Table S1. This value is comparable to LOD reported for other cortisol FET and CNT-based biosensors.[41,42,57]
As discussed above, the response recorded for the biosensor (S) is a sum of contributions due to specific and non-specific interaction of cortisol with the antibodies functionalized gate electrode. Given that the non-specific contribution is smaller than the specific one and basically constant in the 10 pM–100 nM concentration range, it can be treated as an additive independent contribution that can be subtracted from the current response obtained with the functionalized gate. Therefore, to obtain a calibration curve free of non-specific effects, a second calibration curve was calculated by taking the difference (ΔS) of the signal obtained for each standard sample and the signal obtained for the control gate experiment at the same cortisol concentration. The calibration curve obtained with ΔS is shown in Figure 6b and, as expected, the signal difference tends to increase up to a cortisol concentration of 1 nM, and then, the signal tends towards saturation. With this procedure, a sample solution is measured with both the anti-cortisol antibodies functionalized gate electrode and the control gate electrode, and by taking the difference in response ΔS, the genuine dose curve due to the specific recognition of the cortisol is obtained.[58] The cost of this operation is a reduced maximum signal and a slightly reduced sensitivity to variation in cortisol concentration (Figure 6b). However, the biosensor can still be used in the same range as before and allow to compensate for the effect of non-specific interactions on the EGT sensor response.

Conclusion

In conclusion, we proposed a simple, low-cost, and water-based methodology for the fabrication of electrolyte-gated transistors using SWCNTs as semiconducting material. The ability of BSA to bind at the surface of SWCNTs through non-covalent interactions allowed the preparation of stable dispersion of nanotubes in water, which was then deposited on the substrate to form the transistor channel. The fabricated EGT showed high transconductance and overall good electric properties, whereas here, we demonstrated their application as biosensors for the detection of cortisol in aqueous solutions upon functionalization of the gate electrode with anti-cortisol antibodies. The biosensor allowed the quantification of cortisol in solution between 10 pM and 1 nM, with an estimated LOD of 0.6 pM. Furthermore, having validated the possibility to perform biosensing in solution with this type of devices, this work opens the possibility of using the SWCNTs/BSA hybrids as a basis for a more general biosensing platform where different biological targets can be specifically sensed *via* appropriate gate electrode biofunctionalization protocols.

Experimental Section

Materials: Single-walled semiconducting carbon nanotube (95% *w*/*w*), enriched in (6,5) chirality (45% *w*/*w*), produced using CHASM's patented CoMoCAT™ synthesis method and BSA protein were obtained from Sigma-Aldrich. Cortisol powder and mouse monoclonal recombinant anti-cortisol antibody (ab1949) were purchased from Abcam and used without further purification. The monoclonal antibodies were diluted with phosphate buffer 50 mM pH 7.4 in single use aliquots and stored at –20 °C.

Preparation of SWCNT/BSA dispersions: To prepare the SWCNT/BSA dispersions, 1.5 mg of SWCNTs powder were added to a 3 mg/mL BSA solution in water (1 mL). The mixture was sonicated for 2 h in an ice bath with a tip-probe sonicator (Hielscher Ultrasonic Processor UP200St, equipped with a sonotrode S26d7, used at 30% of the maximum amplitude). The resulting dark-grey dispersion of SWCNTs was centrifuged for 15 min at 14000 x *g* to remove un-dispersed solid. The obtained supernatant, containing the (6,5) SWCNTs/BSA dispersions, was further sonicated for 30 minutes and used to fabricate the transistor devices. The solution was stored at +4 °C.

Devices Fabrication: The test patterns are characterized by four interdigitated electrode pairs with channel L= 15 μm and W/L = 2000 patterned by photolithography and lift-off were purchased from "Fondazione Bruno Kessler" (FBK, Trento, Italy). The electrodes are made of 5 nm thick gold, attached by a few nm chromium adhesive layer to a quartz substrate. The test patterns were cleaned by rinsing with acetone to remove the protective photoresist layer, then sonicated for 5 min in acetone and 5 min in H_2O and dried with nitrogen flow.

A 10 μL drop of SWCNTs/BSA dispersion was drop-cast into the substrate, and the water was evaporated in air. The substrate was then rinsed with H_2O to remove excess material on the surface. A PDMS pool was attached on the substrate to contain the liquid electrolyte/sample and a gold wire electrode was then inserted in the electrolyte solution with a top-gate bottom contact configuration to complete the electrolyte-gated transistor.

Gate Functionalization: A Polycrystalline gold wire was used as a gate electrode and it was cleaned through immersion in KOH 2.5 M at 110 °C for 4 hours, followed by immersion in concentrated H_2SO_4 at 220 °C for 2 hours and a final rinse with H_2O. Cortisol antibodies were immobilized on the gold gate surface according to the following protocol: (i) a first overnight incubation step in mixture of SAM-forming molecules (11-mercaptoundecanoic acid: 6-mercaptohexanol 1:3 molar ratio, in ethanol) at room temperature; (ii) immersion in a solution of 20 mM *N*-(3-dimethylaminopropyl)-*N*-ethylcarbodiimidehydrochloride (EDC) and 50 mM *N*-hydroxysuccinimide (NHS) in MES buffer 100 mM pH 6.0; (iii) incubation in a 0.1 mg/mL^{-1} of cortisol monoclonal antibodies in phosphate buffer 50 mM pH 7.4 for 2 hours; (iv) immersion in 50 mM ethanolamine (ETA) in in phosphate buffer 50 mM PBS pH 7.4, for 30 min. For the control experiments, the Au gate was functionalized with antibodies nonspecific for cortisol; monoclonal antibodies for prolactin induced protein were used in this study. The gate electrode functionalization was performed *ex situ* as a separate step, before the assembling of the transistor device, in order to avoid potential activation of carboxylic acid defects present on the nanotubes surface by the EDC/NHS reactant solution.

UV-vis and Raman Spectroscopy: UV-vis absorption spectra of the SWCNTs/BSA solution were recorded at room temperature with a Varian Cary 50 spectrophotometer.

Raman spectra were recorded using an Horiba Scientific LabRam HR Evolution at room temperature using a 633 nm laser source. The laser was operated at 25% power. The Raman spectra were acquired directly on the interdigitated drain/source electrodes, after the formation of the SWCNT/BSA random network. To ensure acceptable measurement statistics, ~25 spectra were collected per sample tested. The spectra were processed (normalized, averaged) and then analysed.

Atomic Force Microscopy: The SWCNTs/BSA dispersion was deposited on an IDE test pattern and imaged in air by a NT-MDT SMENA Solver platform (Moscow, Russia) operated in semi-contact mode. Images were collected at an average scan frequency of 1 line/s using NTMDT NSG10 tips with a nominal spring constant of 12 N/m. The images have been analysed using Gwyddion 2.56 freeware (http://gwyddion.net).

Electrochemical characterization: The gate electrode functionalization was characterized by cyclic voltammetry (CV) and electrochemical impedance spectroscopy (EIS), using a CH Instrument potentiostat 760c model. After each functionalization step, both CV and EIS measurements were carried out using a three-electrode setup. The gate electrode was used as a working electrode, whereas a Pt wire and an Ag/AgCl electrode were chosen as counter electrode and reference electrode, respectively.

The CV characterization was performed in a 5 mM $K_3[Fe(CN)_6]$, 1 M KCl aqueous solution. The faradaic current was recorded scanning from –0.2 V to +0.6 V *vs* Ag/AgCl, with a scan rate of 0.050 V s^{-1}. EIS spectra were collected in a 5 mM $K_3[Fe(CN)_6]$, 1 M KCl electrolyte solution at an initial potential of 0.270 V, with an AC amplitude of 0.005 V and a frequency range from 0.1 Hz to 10 kHz. The results were reported in form of Nyquist plots by reporting the imaginary component (–Z") vs the real component (Z') of the recorded impedance.

Electrical Characterization and Biosensing: Electrical characterization was performed in phosphate buffer 50 mM, pH 7.4 with a Au wire gate electrode. Source, drain, and gate electrodes were connected to an Agilent B2912A Source Meter Unit. All measurements were carried out at room temperature. The *I*–*V* transfer characteristics were recorded by sweeping the gate-source voltage (V_{GS}) from 0.0 V to −0.8 V (sweep rate 20 mV s^{-1}) with a fixed drain-source voltage (V_{DS}) constant at −0.050 V (transistor linear regime). The output characteristics were recorded by sweeping V_{DS} from 0.0 V to −0.5 V and V_{GS} from 0 V to –0.8 V with steps of 0.2 V. Before performing the biosensing experiments, each EGT device was stabilized by recording consecutive transfer curves at 5 min interval between each other, until I_{DS} stability.

Cortisol biosensing measurements were performed by using buffered solutions with increasing concentrations of cortisol (from 1 pM to 1 µM) as the gating electrolyte. For each sample solution, transfer curves were recorded continuously by sweeping the gate-source voltage (V_{GS}) from 0.0 V to −0.8 V (sweep rate 20 mV s^{-1}), with a fixed drain-source voltage V_{DS} = −0.050 V, until stabilization of the I_{DS} current. To quantify the device response to the analyte, the signal S was defined as $S = (I–I_0)/I_0$, where I is the current recorded at V_{GS}= –0.8 V for a particular sample and I_0 is the relative current in the absence of cortisol. Cortisol standard solutions were obtained by preparing a fresh 150 µM cortisol stock solution in 20% *v*/*v* N,N-dimethylformamide, 80% *v*/*v* phosphate buffer 50 mM pH 7.4; the standard samples were prepared by diluting this solution with phosphate buffer 50 mM pH 7.4 at the target concentration. **I**

Computational details: Docking models of the interaction between BSA and (6,5) SWCNT were obtained by using the PatchDock algorithm. The ff14SB force field was used to model the BSA, while the CNT atoms were modelled by using the ca atom type (sp2 aromatic carbon parameter), from the gaff force field. Simulations were performed with explicit solvent by using the TIP3P water model. Counterions were included to neutralize the total charge of the system. MM and MD simulations were carried out using AMBER 16. The initial docked poses were minimized, the solvated systems were equilibrated and then, 100 ns long MD simulations were produced. Particle Mesh Ewald summation was used throughout (cut off radius of 10 Å for the direct space sum). H-atoms were considered by the SHAKE algorithm and a time step of 2 fs was applied in all MD runs. The molecular mechanics–generalised Born surface area (MM-GBSA) method was applied to compute the binding energy between BSA and the (6,5) SWCNT in the different positions, extracting 1000 snapshots from each MD trajectory. An infinite cut-off was used for all the interactions. The electrostatic contribution to the solvation free energy was calculated using the generalized Born (GB) model (igb = 5), as implemented in MMPBSA.py. The non-polar contribution to the solvation free energy was determined using solvent-accessible, surface-area-dependent terms. The per-residue decomposition of $\Delta E_{binding}$ (fingerprint analysis) was obtained by MMPBSA.py.

Acknowledgements

We are grateful to Professor Maurizio Prato for inspiring us and many others with his pioneering work on carbon allotropes as functional materials for bio-interphases. This work is supported by the Italian Ministry of Foreign Affairs and International Cooperation and by the Israeli Ministry of Science and Technology (grant agreement number 3-17367). C.A.B and M.B. acknowledge University of Modena and Reggio Emilia through 'FAR 2021' Fondazione di Modena, and Life Science Department respectively, for funding.

Conflict of Interest

The authors declare no competing financial interest.

Keywords: Antibodies • BSA • Cortisol • EGT • Nanotubes

[1] F. Torricelli, D. Z. Adrahtas, Z. Bao, M. Berggren, F. Biscarini, A. Bonfiglio, C. A. Bortolotti, C. D. Frisbie, E. Macchia, G. G. Malliaras, I. McCulloch, M. Moser, T.-Q. Nguyen, R. M. Owens, A. Salleo, A. Spanu, L. Torsi, *Nat. Rev. Methods Primers* **2021**, *1*, 66.

[2] X. Liu, L. Huang, K. Qian, *Adv. Nanobiomed Res.* **2021**, *1*, 2000104.

[3] O. Zohar, M. Khatib, R. Omar, R. Vishinkin, Y. Y. Broza, H. Haick, *View* **2021**, *2*, 20200172.

[4] F. Meng, W. Yu, C. Chen, S. Guo, X. Tian, Y. Miao, L. Ma, X. Zhang, Y. Yu, L. Huang, K. Qian, J. Wang, *Small* **2022**, *18*, 2200784.

[5] Y. Wang, P. Tan, Y. Wu, D. Luo, Z. Li, *View* **2022**, *3*, 20220026.

[6] E. Macchia, Z. M. Kovács-Vajna, D. Loconsole, L. Sarcina, M. Redolfi, M. Chironna, F. Torricelli, L. Torsi, *Sci. Adv.* **2022**, *8*, eabo0881.

[7] L. Torsi, M. Magliulo, K. Manoli, G. Palazzo, *Chem. Soc. Rev.* **2013**, *42*, 8612.

[8] B. Shkodra, M. Petrelli, M. A. Costa Angeli, D. Garoli, N. Nakatsuka, P. Lugli, L. Petti, *Appl. Phys. Rev.* **2021**, *8*, 041325.

[9] A. Molazemhosseini, F. A. Viola, F. J. Berger, N. F. Zorn, J. Zaumseil, M. Caironi, *ACS Appl. Electron. Mater.* **2021**, *3*, 3106–3113.

[10] J. M. Schnorr, T. M. Swager, *Chem. Mater.* **2011**, *23*, 646–657.

[11] D. Jariwala, V. K. Sangwan, L. J. Lauhon, T. J. Marks, M. C. Hersam, *Chem. Soc. Rev.* **2013**, *42*, 2824–2860.

[12] A. D. Franklin, M. C. Hersam, H. S. P. Wong, *Science* **2022**, *378*, 726–732.

[13] B. L. Allen, P. D. Kichambare, A. Star, *Adv. Mater.* **2007**, *19*, 1439–1451.

[14] D. Tasis, N. Tagmatarchis, V. Georgakilas, M. Prato, *Chem. – Eur. J.* **2003**, *9*, 4000–4008.

[15] S. Reich, C. Thomsen, P. Ordejón, *Phys. Rev. B* **2002**, *65*, 155411.

[16] A. Graf, Y. Zakharko, S. P. Schießl, C. Backes, M. Pfohl, B. S. Flavel, J. Zaumseil, *Carbon* **2016**, *105*, 593–599.

[17] B. S. Flavel, K. E. Moore, M. Pfohl, M. M. Kappes, F. Hennrich, *ACS Nano* **2014**, *8*, 1817–1826.

[18] F. Bottacchi, L. Petti, F. Späth, I. Namal, G. Tröster, T. Hertel, T. D. Anthopoulos, *Appl. Phys. Lett.* **2015**, *106*, 193302.

[19] C. S. Lee, R. E. A. Gwyther, M. Freeley, D. Jones, M. Palma, *ChemBioChem.* **2022**, *23*, e202200282.

[20] Y. L. Zhao, J. F. Stoddart, *Acc. Chem. Res.* **2009**, *42*, 1161–1171.

[21] X. Xu, P. Clément, J. Eklöf-Österberg, N. Kelley-Loughnane, K. Moth-Poulsen, J. L. Chávez, M. Palma, *Nano Lett.* **2018**, *18*, 4130–4135.

[22] E. Anaya-Plaza, A. Shaukat, I. Lehtonen, M. A. Kostiainen, *Adv. Healthcare Mater.* **2021**, *10*, 2001162.

[23] M. Di Giosia, F. Valle, A. Cantelli, A. Bottoni, F. Zerbetto, E. Fasoli, M. Calvaresi, *Carbon* **2019**, *147*, 70–82.

[24] M. Calvaresi, F. Zerbetto, *Acc. Chem. Res.* **2013**, *46*, 2454–2463.

[25] M. Berto, M. Di Giosia, M. Giordani, M. Sensi, F. Valle, A. Alessandrini, C. Menozzi, A. Cantelli, G. C. Gazzadi, F. Zerbetto, M. Calvaresi, F. Biscarini, C. A. Bortolotti, *Adv. Electron. Mater.* **2021**, *7*, 2001114.

[26] X. Xu, B. J. Bowen, R. E. A. Gwyther, M. Freeley, B. Grigorenko, A. V Nemukhin, J. Eklöf-Österberg, K. Moth-Poulsen, D. D. Jones, M. Palma, *Angew. Chem. Int. Ed.* **2021**, *60*, 20184–20189.

[27] G. Bisker, J. Dong, H. D. Park, N. M. Iverson, J. Ahn, J. T. Nelson, M. P. Landry, S. Kruss, M. S. Strano, *Nat. Commun.* **2016**, *7*, 10241.

[28] R. J. Chen, Y. Zhang, D. Wang, H. Dai, *J. Am. Chem. Soc.* **2001**, *123*, 3838–3839.

[29] N. Amdursky, E. D. Głowacki, P. Meredith, *Adv. Mater.* **2019**, *31*, 1802221.

[30] Y. Agam, R. Nandi, A. Kaushansky, U. Peskin, N. Amdursky, *Proc. Natl. Acad. Sci. U. S. A.* **2020**, *117*, 32260–32266.

[31] K. Matsuura, T. Saito, T. Okazaki, S. Ohshima, M. Yumura, S. Iijima, *Chem. Phys. Lett.* **2006**, *429*, 497–502.

[32] A. Clow, F. Hucklebridge, T. Stalder, P. Evans, L. Thorn, *Neurosci. Biobehav. Rev.* **2010**, *35*, 97–103.

[33] P. Restituto, J. C. Galofré, M. J. Gil, C. Mugueta, S. Santos, J. I. Monreal, N. Varo, *Clin. Biochem.* **2008**, *41*, 688–692.

[34] R. Yehuda, M. H. Teicher, R. L. Trestman, R. A. Levengood, L. J. Siever, *Biol. Psychiatry* **1996**, *40*, 79–88.

[35] A. Ganguly, K. C. Lin, S. Muthukumar, S. Prasad, *ACS Sens.* **2021**, *6*, 63–72.

[36] W. Tang, L. Yin, J. R. Sempionatto, J.-M. Moon, H. Teymourian, J. Wang, W. Tang, L. Yin, J. R. Sempionatto, J. Moon, H. Teymourian, J. Wang, *Adv. Mater.* **2021**, *33*, 2008465.

[37] S. Kim, B. Lee, J. T. Reeder, S. H. Seo, S. U. Lee, A. Hourlier-Fargette, J. Shin, Y. Sekine, H. Jeong, Y. S. Oh, A. J. Aranyosi, S. P. Lee, J. B. Model, G. Lee, M. H. Seo, S. S. Kwak, S. Jo, G. Park, S. Han, I. Park, H. Il Jung, R. Ghaffari, J. Koo, P. V. Braun, J. A. Rogers, *Proc. Natl. Acad. Sci. U. S. A.* **2020**, *117*, 27906–27915.

[38] U. Teruhisa, H. Ryoji, I. Taisuke, S. Tatsuya, M. Fumihiro, S. Tatsuo, *Clin. Chim. Acta* **1981**, *110*, 245–253.

[39] R. F. Vining, R. A. McGinley, J. J. Maksvytis, K. Y. Ho, *Ann. Clin. Biochem.* **1983**, *20*, 329–335.

[40] J. Heikenfeld, *Electroanalysis* **2016**, *28*, 1242–1249.

[41] L. Bian, W. Shao, Z. Liu, Z. Zeng, A. Star, *J. Electrochem. Soc.* **2022**, *169*, 057519.

[42] B. Wang, C. Zhao, Z. Wang, K. A. Yang, X. Cheng, W. Liu, W. Yu, S. Lin, Y. Zhao, K. M. Cheung, H. Lin, H. Hojaiji, P. S. Weiss, M. N. Stojanović, A. J. Tomiyama, A. M. Andrews, S. Emaminejad, *Sci. Adv.* **2022**, *8*, 967.

[43] S. M. Bachilo, M. S. Strano, C. Kittrell, R. H. Hauge, R. E. Smalley, R. B. Weisman, *Science* **2002**, *298*, 2361–2366.

[44] M. Brohmann, F. J. Berger, M. Matthiesen, S. P. Schießl, S. Schneider, J. Zaumseil, *ACS Nano* **2019**, *13*, 7323–7332.

[45] A. Jorio, R. Saito, *J. Appl. Phys.* **2021**, *129*, 021102.

[46] M. S. Dresselhaus, G. Dresselhaus, R. Saito, A. Jorio, *Phys. Rep.* **2005**, *409*, 47–99.

[47] M. Di Lauro, M. Berto, M. Giordani, S. Benaglia, G. Schweicher, D. Vuillaume, C. A. Bortolotti, Y. H. Geerts, F. Biscarini, *Adv. Electron. Mater.* **2017**, *3*, 1700159.

[48] M. Dankerl, M. V. Hauf, A. Lippert, L. H. Hess, S. Birner, I. D. Sharp, A. Mahmood, P. Mallet, J.-Y. Veuillen, M. Stutzmann, J. A. Garrido, *Adv. Funct. Mater.* **2010**, *20*, 3117–3124.

[49] D. Heimfarth, M. Balcı Leinen, P. Klein, S. Allard, U. Scherf, J. Zaumseil, *ACS Appl. Mater. Interfaces* **2022**, *14*, 8209–8217.

[50] I. Heller, A. M. Janssens, J. Männik, E. D. Minot, S. G. Lemay, C. Dekker, *Nano Lett.* **2008**, *8*, 591–595.

[51] S. Goutelle, M. Maurin, F. Rougier, X. Barbaut, L. Bourguignon, M. Ducher, P. Maire, *Fundam. Clin. Pharmacol.* **2008**, *22*, 633–648.

[52] M. Berto, S. Casalini, M. di Lauro, S. L. Marasso, M. Cocuzza, D. Perrone, M. Pinti, A. Cossarizza, C. F. Pirri, D. T. Simon, M. Berggren, F. Zerbetto, C. A. Bortolotti, F. Biscarini, *Anal. Chem.* **2016**, *88*, 12330–12338.

[53] P. A. Manco Urbina, M. Berto, P. Greco, M. Sensi, S. Borghi, M. Borsari, C. A. Bortolotti, F. Biscarini, *J. Mater. Chem. C* **2021**, *9*, 10965–10974.

[54] H. Swenson, N. P. Stadie, *Langmuir* **2019**, *35*, 5409–5426.

[55] J. M. Honig, L. H. Reyerson, *J. Phys. Chem.* **1952**, *56*, 140–144.

[56] A. D. McNaught, A. Wilkinson, *IUPAC Compendium of Chemical Terminology, 2nd Ed.*, Blackwell Scientific Publications, Oxford, **1997**.

[57] H.-J. Jang, T. Lee, J. Song, L. Russell, H. Li, J. Dailey, P. C. Searson, H. E. Katz, *ACS Appl. Mater. Interfaces* **2018**, *10*, 16233–16237.

[58] V. Parkula, M. Berto, C. Diacci, B. Patrahau, M. Di Lauro, A. Kovtun, A. Liscio, M. Sensi, P. Samorì, P. Greco, C. A. Bortolotti, F. Biscarini, *Anal. Chem.* **2020**, *92*, 9330–9337.

Entry for the Table of Contents

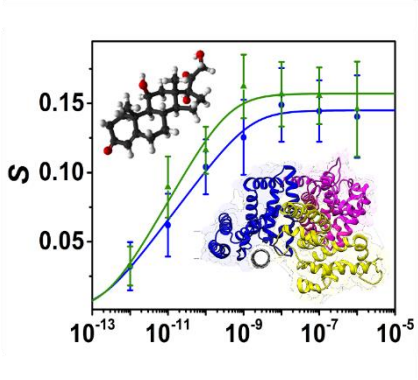

A robust methodology for the fabrication of electrolyte-gated transistor biosensors is presented. Single walled carbon nanotubes are hybridized with bovine serum albumin allowing the transistor fabrication from aqueous solution. The sensor functionality is demonstrated for the detection of cortisol in solution after immobilization of antibodies on the gate surface. Analysis of the signal allows the extraction of binding parameters.